1 **Title:**

2 **Loss of Rnf31 and Vps4b sensitizes pancreatic cancer to T cell-mediated killing**

3

4 **Authors:**

5 Nina Frey[1,2], Luigi Tortola[1], David Egli[1], Sharan Janjuha[2], Kim Fabiano Marquart[1,2], Tanja

6 Rothgangl[2], Franziska Ampenberger[1], Manfred Kopf[1] and Gerald Schwank[1,2]*

7

8 **Affiliations:**

9 [1] Institute of Molecular Health Sciences, ETH Zurich, Zurich, Switzerland

10 [2] Department of Pharmacology and Toxicology, University of Zurich, Zurich, Switzerland

11 *Corresponding author: gerald.schwank@uzh.ch

12

13 **Abstract**:

14 Pancreatic ductal adenocarcinoma (PDA) is an inherently immune cell deprived tumor,

15 characterized by desmoplastic stroma and suppressive immune cells. Here we systematically

16 dissected PDA intrinsic mechanisms of immune evasion by *in vitro* and *in vivo* CRISPR

17 screening, and identified Rnf31 and Vps4b as essential factors required for escaping CD8^{+} T

18 cell-killing. Using murine PDA cells and human PDA organoids, we demonstrate that *Rnf31*

19 protects from TNF-mediated caspase 8 cleavage and subsequent apoptosis induction. For

20 *Vps4b* we found that inactivation impairs autophagy, resulting in increased accumulation of

21 CD8^{+} T cell-derived granzyme B and subsequent tumor cell lysis. Orthotopic transplantation

22 of Rnf31- or Vps4b deficient pancreatic tumors, moreover, revealed increased CD8^{+} T cell

23 infiltration and effector function, and markedly reduced tumor growth in mice. Our work

24 uncovers vulnerabilities in PDA that might be exploited to render these tumors more

25 susceptible to the immune system.

26

27

Introduction:

Immune evasion is a common trait of most human cancers. Through phenotypic changes tumor cells evade recognition of effector T cells and modulate the tumor microenvironment to establish an immune suppressive niche [1,2]. While immune checkpoint inhibition shows great potential for curative cancer treatment, pancreatic ductal adenocarcinoma (PDA) is largely refractory to immunotherapy [3,4]. Among the described mechanisms responsible for the highly effective immune evasion of PDA are (i) insufficient antigenicity [5], (ii) high expression of PD-L1 [6], (iii) exclusion of dendritic cells while attracting T regulatory cells [2] and suppressive myeloid populations [7,8], and (iv) the sequestration of major histocompatibility complex class 1 (MHC-I) [9]. In order to better understand cell-autonomous mechanisms that protect tumors from immune clearance, genome-wide CRISPR-Cas9 screens have been performed in melanoma, renal-, colorectal- and breast cancer cell lines. Together they identified the interferon-ɣ (IFNɣ) response, TNF-mediated NFκB signaling and autophagy as core pathways involved in immune evasion across different cancer types [10–18]. However, to our knowledge, a comprehensive genetic analysis of potential target genes to enhance anti-tumor immunity in PDA is still missing.

Here we used genome-wide *in vitro* CRISPR screening and targeted *in vivo* CRISPR screening to systematically reveal positive and negative regulators of cytotoxic T lymphocyte (CTL) sensitivity in PDA. In addition to previously described genes involved in the regulation CTL-mediated tumor cell killing, we identify *Rnf31* and *Vps4b* as central components for PDA immune escape *in vitro* and *in vivo*. Our results suggest that *Rnf31,* as part of the linear ubiquitination chain assembly complex (LUBAC), mediates immune-escape by stabilizing anti-apoptotic proteins in the TNF pathway, and that *Vps4b,* as part of the autophagy machinery, reduces susceptibility to T-cell mediated tumor cell lysis by lowering intracellular granzyme B contents. The elucidated mechanisms of immune evasion in PDA provide potential strategies for enhancing efficacy of cancer immunotherapies.

Results:

A genome-wide CRISPR screen identifies regulators of immune evasion in PDA

To identify genes modulating CTL-mediated killing of PDA we performed a pooled, genome-wide CRISPR knock-out screen in pancreatic cancer cells. We first engineered a PDA cell line derived from the autochthonous KPC mouse model (*Kras*[G12D], *Trp53*[R172H/+,] *Pdx*-**C**re), which stably expresses *Sp*Cas9 and chicken ovalbumin (OVA). Cells were subsequently transduced

2

61   with a murine single-guide (sg)RNA library targeting 19 647 genes at a 500x coverage [19]. To

62   mimic cytotoxic T cell killing, we co-cultured cancer cells for three days with activated, OVA-

63   specific CD8+ T cells (OT-I T cells), followed by a three-day recovery period prior to DNA

64   isolation for analysis by next generation sequencing (NGS) from the surviving cell population

65   [Fig. 1a]. Validating screening conditions and sufficient library representation, we observed a

66   strong overlap of depleted sgRNAs targeting essential genes in OT-I T cell treated- and

67   untreated KPC cells [Supplementary Figs. 1a, b]. Next, we inspected differentially distributed

68   sgRNAs, and defined genes targeted by enriched sgRNAs as resistors and genes targeted by

69   depleted sgRNAs as sensitizers for CTL-mediated killing (FDR < 0.1). We identified several

70   genes with a well-characterized role in CTL-mediated killing in different cancer types,

71   demonstrating that the previously described core cancer intrinsic CTL evasion gene network is

72   also conserved in PDA [Figs. 1b, c] [10–12,14,20]. For example, genes associated with the IFNɣ

73   pathway (*Jak1*, *Jak2*, *Ifngr1*, *Ifngr2*, *Stat1)* and antigen presentation machinery (*B2m*, *Tap1*)

74   conferred resistance to CTL-mediated PDA killing upon inactivation [Figs. 1c, d,

75   Supplementary Fig. 1c], and genes regulating TNF-triggered apoptosis (*Cflar*, *Traf2*), NFκB

76   signaling (*Nfkbia*, *Tnfaip3*) and autophagy (*Atg5*, *Atg7*, *Atg10*, *Atg12*, *Gabarapl2*) sensitized

77   PDA cells to CTL-mediated killing upon inactivation [Figs. 1c, d, Supplementary Fig. 1c].

78   Interestingly, the two strongest sensitizers to T cell-mediated killing identified in our PDA

79   screen were *Rnf31* and *Vps4b,* but for both genes mechanistic insights in context of CTL

80   sensitivity are lacking.

81

82   **A targeted CRISPR screen validates immune modulators *in vivo***

83   To explore whether top candidates from the *in vitro* screen also affect CTL-mediated PDA

84   killing *in vivo* we next performed a targeted library screen in mice. We generated a secondary

85   library targeting 63 genes (hits with FDR < 0.1) with ten sgRNAs per gene, and containing 600

86   non-targeting control sgRNAs as well as seven positive control sgRNAs targeting ovalbumin.

87   We furthermore omitted several IFNɣ pathway components to avoid redundancy. The library

88   was transduced into KPC-Cas9-OVA cells, which we subsequently orthotopically transplanted

89   into pancreata of RAG1-/- mice. After tumor formation, we adoptively transferred activated

90   CD8+ OT-I T cells to tumor-bearing mice and collected the residual tumors five days later [Fig.

91   2a]. In vivo validated candidates showed consistent phenotypes across all mice [Fig. 2b], and

92   in line with previous studies we observed a substantial, albeit not complete overlap between *in*

93   *vitro* and *in vivo* screening results [Fig. 2c, Supplementary Fig. 2a] [21]. Resistors of CTL evasion

94   included well-known immune evasion genes, such as *Stat1* and *Casp8,* as well as the positive

95   control *ovalbumin* [Fig. 2b]. Among sensitizers of CTL killing - which are of particular

96   therapeutic interest as they bear the potential to enhance anti-tumor immunity in PDA upon

97   inhibition - were the previously described genes *Adar* and *Cflar* [22–24], as well as the two

98   strongest sensitizers identified in our CRISPR screen, *Vps4b* and *Rnf31* [Figs. 2b, d], prompting

99   us to further study their role in PDA immune evasion.

100

101   **A competition assay confirms the role of *Rnf31* and *Vps4b* in immune evasion**

102   We then performed arrayed validation of *Vps4b-* and *Rnf31*-mediated PDA sensitization to

103   CTL killing in a competition assay. KPC-Cas9-OVA cells carrying *Vps4b-* and *Rnf31*-

104   targeting sgRNAs were labeled with mCherry$^+$, and KPC-Cas9-OVA cells carrying a non-

105   targeting control sgRNA were labeled with GFP$^+$. After confirming that knock-outs do not

106   affect cell proliferation per-se [Supplementary Fig. 3a], we co-cultured candidate lines with

107   CD8$^+$ OT-I T cells and assessed mCherry and GFP proportions by flow cytometry [Fig. 3a].

108   As expected, without generating a gene knock-out in mCherry$^+$ cells we did not observe a shift

109   in the mCherry:GFP ratio after the addition of OT-I T cells [Figs. 3b, c], while targeting *Stat1,*

110   a well-known resistor of CTL killing and positive control for our assay, shifted the ratio

111   towards IFNɣ- signaling deficient mCherry$^+$ cells [Figs. 3b, c]. In contrast, *Vps4b*^{KO} and

112   *Rnf31*^{KO} KPC cells had a strong growth disadvantage under immune attack, leading to an

113   increase of the GFP$^+$ control cell population [Figs. 3b, c]. Our results therefore confirm that

114   inhibition of *Rnf31* and *Vps4b* sensitizes PDA to CTL killing.

115

116   **Functional characterization of the role of *Rnf31* and *Vps4b* in immune evasion**

117   Antigen presentation by major histocompatibility complex I (MHC-I) proteins is necessary for

118   efficient anti-tumor immunity. As shown in a recent study, pancreatic cancer cells commonly

119   sequestrate MHC-I to evade the adaptive immune system [9], prompting us to suspected that loss

120   of *Rnf31* and *Vps4b* facilitates CD8$^+$ mediated killing by increasing MHC-I levels on PDA. To

121   test this hypothesis, we assessed surface MHC-I levels in KPC cells upon exposure to CTLs.

122   Confirming our assay, we observed robust induction of MHC-I upregulation in parental KPC

123   cells, which, as expected, was perturbed in IFNɣ signaling deficient *Stat1*^{KO} cells (Fig. 3d,

124   Supplementary Fig. 3d). Next, we analyzed MHC-I induction in *Rnf31*^{KO} and *Vps4b*^{KO} KPC

125   cells. However, we observed similar surface MHC-I levels compared to the parental cell line

126   (Fig. 3d), demonstrating that enhanced CTL-mediated killing is not triggered by an increase in

127   antigen presentation [Fig. 3d].

128   Next, we sought to gain insights into the transcriptional networks mediating the sensitizing

129   effects of *Rnf31*[KO] and *Vps4b*[KO] to CTL killing. We therefore performed RNA-sequencing

130   (RNA-seq) on the different PDA knock-out lines with and without six hours of CD8^{+} T cell

131   exposure [Supplementary Fig. 3b]. Confirming functional gene knock-outs, transcript levels of

132   *Rnf31* and *Vps4b* were downregulated in the respective PDA lines [Supplementary Fig. 3c].

133   Furthermore, *Rnf31*[KO] and *Vps4b*[KO] cell lines displayed relatively mild, but consistent

134   transcriptional changes [Fig. 3e]. Among the differentially expressed genes in CTL-treated

135   *Rnf31* or *Vps4b* knock-out PDA cells were several cytokines and chemokines, including the

136   Cxcr3 ligands *Cxcl9/10/11* [Figs. 3e, f]. Notably, the Cxcr3-Stat3 signaling axis has previously

137   been described to enhance PDA aggressiveness and contribute to an immune suppressive

138   environment through inducing PD-L1 (CD274) expression [25,26], and low expression of these

139   chemokines is correlated with a better prognosis in human PDA patients [Supplementary Fig.

140   3e]. We therefore hypothesize that downregulation of Cxcr3 ligands contributes to the immune

141   stimulatory environment triggered by *Rnf31* and *Vps4b* inactivation.

142

143   **Rnf31 loss sensitizes PDA to TNF- induced apoptosis via caspase 8**

144   Cytotoxic T cells induce death in target cells via different processes, including the release of

145   TNF, secretion of granules filled with granzymes and perforins, and by engaging the Fas-FasL

146   axis. To systematically explore which of these effector mechanisms are sensitized upon *Rnf31*

147   and *Vps4b* inhibition, we first assessed tumor cell sensitivity to TNF ligands. Interestingly, we

148   found that parental KPC cells and *Vps4b*[KO] KPC cells were insensitive to TNF-induced

149   apoptosis, but that *Rnf31*[KO] KPC cells rapidly underwent cell death upon TNF treatment [Fig.

150   4a]. Engagement of the TNF receptor triggers several signaling branches, including pro-

151   survival NFκB signaling as well as apoptosis induction via caspase 8 cleavage [27–29]. Notably,

152   *Rnf31* has previously been reported to function as an E3 ubiquitin-protein ligase within the

153   linear ubiquitination chain assembly complex (LUBAC), which is involved in regulating NFκB

154   signaling and in stabilizing anti-apoptotic proteins such as c-Flip [27]. We therefore speculated

155   that the *Rnf31* knock-out sensitizes tumor cells to TNF-mediated apoptosis either indirectly, by

156   abrogating NFκB pro-survival signaling, or directly, by facilitating caspase 8 cleavage. When

157   we first assessed TNF-mediated NFκB activation, we found phosphorylation of the NFκB

158   subunit p65/Rela in all genetic backgrounds, including *Rnf31*[KO] cells [Fig. 4b], indicating

5

159 functional NFκB signaling. When we next analyzed caspase 8 cleavage upon TNF treatment,

160 activation was observed in *Rnf31*[KO] KPC cells but not in parental KPC- or *Vps4b*[KO] KPC cells

161 [Fig. 4b]. Hence, our data suggest that in Rnf31-deficient cells intact NFκB signaling is not

162 sufficient to rescue TNF-activated caspase 8 cleavage.

163 To further assess whether loss of Rnf31 also sensitizes human PDA to TNF-mediated cell

164 death, we next generated patient-derived and engineered human pancreatic cancer organoids

165 (hPDA) with *RNF31*[KO] mutations, and treated these organoids for four hours with TNF. In line

166 with results from murine PDA tissues, only *RNF31*[KO] but not *RNF31*[WT] PDA organoids

167 activated apoptotic cell death upon TNF stimulation [Figs. 4c, d, Supplementary Figs. 4a, b].

168 Taken together, our results suggest that loss of the LUBAC subunit Rnf31 sensitizes murine

169 and human pancreatic cancer to CTL killing by rendering cells susceptible to caspase-8-

170 mediated apoptosis upon TNF signaling [Supplementary Fig. 4c].

171

172 **Vps4b depletion impairs functional autophagy and increases intracellular Granzyme B**

173 **levels**

174 As part of endosomal sorting complexes required for transport III (ESCRT-III) Vps4b

175 functions as an AAA-type ATPase involved in diverse processes regulating protein

176 homeostasis, including the catalyzation of phagophore closure during autophagy [30].

177 Considering that several autophagy-related genes have been identified as sensitizers for CTL-

178 mediated killing, we reasoned that *Vps4b*[KO] cells might sensitize PDA to CTL-killing by

179 inhibiting autophagy. To test this hypothesis, we transduced cells with an autophagic flux

180 reporter, and assessed if autophagy is impaired in *Vps4b* knock-out KPC cells [31]. The reporter

181 consists of a LC3-GFP-LC3ΔG-RFP fusion protein; LC3-GFP is localized to the

182 autophagosome and degraded during autophagy, and LC3ΔG-RFP lacks a C-terminal glycine

183 and stably resides in the cytoplasm during autophagy [Fig. 5a]. While parental KPC cells

184 showed a strong upregulation of autophagy upon starvation [Fig. 5b], *Vps4b*[KO] KPC cells

185 showed an impaired autophagic flux, similar to fully autophagy-deficient *Atg5*[KO] KPC cells

186 [Fig. 5b]. These data suggest that loss of Vps4b sensitizes PDA to CTL killing through

187 disrupting autophagy.

188 In a previous study it was suggested that high autophagy rates in PDA contribute to immune

189 evasion by sequestering surface MHC-I levels [9]. In KPC cells, nevertheless, we observed a

190 robust induction of MHC-I surface expression upon CTL exposure, which was also not affected

191 by Vps4b depletion (Fig. 3d). In another model it was suggested that autophagy inhibition

6

192 facilitates CTL-mediated killing through increasing sensitivity to TNF-induced cell death [11].
193 However, we did not observe apoptosis induction when we treated Vps4b[KO] KPC cells with
194 TNF [Fig. 4a]. In addition, when we sensitized KPC cells to TNF-induced apoptosis through
195 Actinomycin D - a transcriptional inhibitor of pro-survival NFκB signaling - prior to TNF
196 treatment, *Vps4b*[KO] KPC cells were again not sensitized to increasing TNF concentrations
197 compared to parental KPC cells [Fig. 5c]. Interestingly, a recent studies found that high
198 autophagy levels in breast cancer cells promote NK cell-derived granzyme B degradation,
199 resulting in resistance to cytotoxic immune cells [32,33]. We therefore hypothesized that autophagy
200 deficiency could sensitize PDA cells to CTL killing through insufficient granzyme B clearance.
201 Hence, we quantified intracellular granzyme B levels in KPC cells upon OT-I T cell exposure.
202 Indeed, while OT-I T cells produced comparable amounts of granzyme B, autophagy deficient
203 *Atg5*[KO]- and *Vps4b*[KO] KPC cells accumulated more granzyme B compared to parental KPC cells
204 [Figs. 5d, e, Supplementary Fig. 5a]. Taken together, our data suggest that *Vps4b* inhibition
205 perturbs autophagy and thereby reduces the capability of PDA cells to degrade granzyme B
206 upon CTL-mediated killing. Importantly, this phenotype was not only limited to *Vps4b*-
207 deficient cells, but generally linked to PDA cells with impaired autophagy, providing a model
208 how autophagy influences sensitivity to CTL-mediated killing.

209

210 ***Rnf31* and *Vps4b* inhibition increases CTL infiltration and effector function in vivo**
211 To further characterize increased CTL susceptibility of *Rnf31*[KO] and *Vps4b*[KO] KPC cells *in vivo*,
212 we next analyzed the effect of these mutations on PDA progression and tumor
213 microenvironment in mice. Therefore, we orthotopically transplanted KPC cells with different
214 genotypes (wildtype, *Rnf31*[KO] and *Vps4b*[KO]) into C56BL/6 animals, and assessed survival and
215 tumor weight, as well as immune cell composition and effector function using flow cytometry
216 [Fig. 6a, Supplementary Fig. 6d]. While remaining Cas9 expression in these lines did not affect
217 tumor growth [Supplementary Fig. 6a], loss of *Rnf31* and *Vps4b* markedly decreased tumor
218 mass and resulted in significantly enhanced survival of tumor-bearing mice [Fig. 6b]. In case
219 of *Vps4b*[KO] tumors the effect was strongly dependent on adaptive immunity, since tumor mass
220 reduction was not apparent in RAG1^{-/-} mice [Supplementary Fig. 6b]. *Rnf31*[KO] tumors,
221 however, also showed reduced growth compared to KPC[WT] tumors in RAG1-deficient hosts,
222 most likely due to the continued expression of TNF and other death receptor ligands by NK
223 cells [Supplementary Fig. 6b]. We next analyzed immune cell infiltration and CD8^{+} T cell
224 effector function across the different tumor genotypes. While loss of *Vps4b* and *Rnf31* did not

225 cause significant changes in macrophages, CD11c+ dendritic cells, CD4+ T helper cells, NK

226 cells and CD4+ Foxp3+ regulatory T cells, we detected a minor increase of neutrophils in

227 *Rnf31*^{KO} tumors [Fig. 6c, Supplementary Fig. 6c]. In addition, we observed a substantial

228 increase of infiltrating CD8+ T cells in *Vps4b*^{KO} and *Rnf31*^{KO} tumors compared to parental KPC

229 tumors [Fig. 6c]. Further analysis of CD8+ CTL markers for effector function revealed a

230 significant reduction in exhausted PD1+ CD8+ T cells in *Vps4b*^{KO} and *Rnf31*^{KO} tumors [Fig. 6d],

231 concomitant with an increase in cytokine production; in *Rnf31*^{KO} tumors TNF production and

232 in *Vps4b*^{KO} tumors TNF and IFNɣ production was increased in infiltrating CD8+ T cells [Fig.

233 6d]. Together, these findings demonstrate that loss of *Rnf31* and *Vps4b* sensitize PDA to CTL-

234 mediated killing also in a non-cell-autonomous manner, through increasing CTL effector

235 function, thereby feeding into a forward loop with cell-autonomous mechanisms to enhance

236 anti-tumor immunity.

237

238 **Discussion**:

239 Several recent studies performed CRISPR screening in PDA to study metastasis formation,

240 metabolic vulnerabilities, combinatorial drug targeting and therapy resistance [21,34–36]. Here, we

241 applied *in vitro* and *in vivo* CRISPR screening in PDA to interrogate tumor intrinsic

242 mechanisms of immune evasion. One of the strongest sensitizers to CTL-mediated killing was

243 *Rnf31,* for which we show that its inactivation facilitates TNF-induced apoptosis via caspase 8

244 cleavage. Notably, previous work has already linked TNF resistance to immune evasion [11,37].

245 However, these studies have been conducted in a TNF-susceptible colorectal cancer cell line

246 (MC38), impeding the identification of TNF sensitizers such as *Rnf31*. In contrast, KPC

247 pancreatic cancer cells are intrinsically resistant to TNF, which allowed us to unravel a

248 mechanism that abates TNF resistance.

249 Another strong sensitizer to CTL-mediated killing identified in our screen was *Vps4b,* which

250 could be linked to autophagy. Autophagy has recently been postulated as an important

251 modulator of anti-tumor immunity in several cancer entities [9–11,38]. However, in contrast to

252 previous findings we did not observe increased MHC-I antigen presentation [9] or enhanced

253 TNF-induced apoptosis [10,11] upon autophagy inhibition. Instead, we provide evidence that

254 impaired autophagy leads to reduced granzyme B clearance, suggesting that *Vps4b* or *Atg5*

255 depletion facilitates tumor cell lysis by CD8+ T cells through enhanced granzyme B

256 accumulation.

257   Taken together, we used functional genomics approaches to identify mechanisms for

258   circumventing immune evasion in PDA. Analysis of two of the strongest hits, *Vps4b* and *Rnf31*,

259   demonstrated that their inhibition sensitizes tumor cell clearance directly, via cell-autonomous

260   mechanisms, and indirectly, by increasing the number and functionality of intertumoral CD8^{+}

261   T cells. Our insights in sensitizing pancreatic cancer to the host immune system could open up

262   novel strategies to enhance the efficacy of T cell-mediated tumor killing, potentially allowing

263   PDA patients to benefit from the vast advances made in the field of cancer immunotherapy in

264   the future.

Methods:

Animals:

Wildtype C57/BL6 mice were obtained from Charles River Laboratories. RAG1$^{-/-}$ (NOD.129S7(B6)-*Rag1*^{tm1Mom}/J) and OT-I (C57BL/6-Tg(*TcraTcrb*)1100Mjb/J) were obtained from Jackson Laboratories and bred in-house. All animals were housed in a pathogen-free animal facility in cages with up to five animals at the Institute of Molecular Health Sciences at ETH Zurich and kept in a temperature- and humidity-controlled room on a 12h light–dark cycle. All animal experiments were performed in accordance with protocols approved by the Kantonales Veterinäramt Zurich in compliance with all relevant ethical regulations.

Cell culture:

The KPC cell line (C57/BL6 background) was generated by Dr. Jen Morton (Beatson Institute) and purchased at Ximbio (Cat# 153474). KPC cells were derived from primary KPC tumors obtained from Pdx-Cre; Kras$^{G12D/+}$; Trp53$^{R172H/+}$ mice. All KPC lines used in this study were cultured in Iscove's Modified Dulbecco's Medium (IMDM, 31980030, Gibco) supplemented with 10% fetal bovine serum (FBS), 1% penicillin/streptomycin (Gibco) and 50 μM β-Mercaptoethanol (Gibco). Cells were incubated at 37°C in 5% CO_2. The parental KPC line was engineered with Lenti-Cas9-Hygromycin and Lenti-Ovalbumin-mCherry-Blasticidin constructs (for details see "Plasmids") in order to express Cas9 and full-length Ovalbumin (KPC-Cas9-OVA).

Plasmids:

For generation of Lenti-EF1α-Cas9-P2A-HygromycinR we replaced Blasticidin from the original vector (Addgene #52962) by HygromycinR using Gibson Assembly. For generation of Lenti-EF1α-Ovalbumin-P2A-mCherry-P2A-BlasticidinR, we replaced Cas9 (Addgene #52962) by Ovalbumin-P2A-mCherry derived from the original vector (Addgene #113030) with Gibson Assembly. The LC3-GFP-LC3ΔG-RFP construct was obtained from Addgene (#84572) and cloned into Lenti-EF1α-Cas9-P2A-BlasticidinR by replacing Cas9-P2A-BlasticidinR. The following vectors LentiGuide-Puro (#52963), LentiCRISPRv2-puro (#98290) and pLenti-PGK-Hygro-KRAS(G12V) (#35635) were obtained from Addgene.

Lentivirus production:

298   For lentivirus production of CRISPR libraries, transgenes or single guide HEK293T cells were

299   transfected with, HEK293T cells (ATCC) were seeded in T175 cell culture flasks in DMEM

300   (Gibco) supplemented with 10% FBS and 1% Penicillin/Streptomycin and grown up to 70%

301   confluency. HEK293T cells were transfected with the following mixture: 10.4 μg psPAX2-

302   Plasmid, 3.5 μg pMD2.G, 13.8 μg lentiviral vector of interest (see section "Plasmids") in a

303   volume of 1000 μl Opti-MEM (Gibco) in tube 1. In a second tube, 138 μl 1mg/mL PEI

304   (Polysciences) was mixed with 862 μl Opti-MEM. Both tubes were incubated at room

305   temperature for 5 min, mixed, and incubated again 20 min at room temperature and added to

306   the cells in the evening. The next morning, medium was refreshed. After 48h and 72h, the

307   supernatant was harvested, filtered with 0.45 μm syringe filters (Sarstedt) and concentrated by

308   centrifugation at 24,000 g for 2h. Plasmids psPAX2 (Addgene #12260) and pMD2.G (Addgene

309   #12559) were gifts from Didier Trono.

310

311   Genome wide CRISPR screen:

312   The genome-wide Brie CRISPR-KO library (4 sgRNAs per gene; ~ 80.000 sgRNAs) was

313   purchased from Addgene (#73632) and amplified according to the supplier's protocol. KPC-

314   Cas9-OVA were infected with the lentiviral Brie CRISPR-KO library at a multiplicity of

315   infection (MOI) of 0.3 while keeping a 500x coverage of the library. One day post transduction,

316   cells were selected with 2 μg/ml Puromycin for 5 days in order to select for successfully

317   transduced cells and to allow gene CRISPR-mediated gene knockout. For OT-I T-cell co-

318   culture, $4x10^7$ KPC cells were plated at a final confluency around 60% and incubated for 3

319   days together with activated T-cells at an E:T ratio of 1:1. After T-cell killing, surviving KPC

320   cells were left to recover for another 3 days. Untreated KPC-Cas9-OVA-Brie cells were

321   cultured alongside and harvested for DNA isolation together with OT-I treated cells. For each

322   replicate and sample, DNA was isolated from $4x10^7$ KPC cells using the Blood & Cell Culture

323   DNA Maxi Kit (Qiagen). NGS libraries were prepared using the following primers:

324   Staggered P5 forward primer:

325   5'AATGATACGGCGACCACCGAGATCTACACTCTTTCCCTACACGACGCTCTTCCG

326   ATCT[N_{1-8}]T TGTGGAAAGGACGAAACACCG

327   Barcoded P7 reverse primer:

328   5'CAAGCAGAAGACGGCATACGAGATNNNNNNNNGTGACTGGAGTTCAGACGTG

329   TGCTCTT CCGATCTTCTACTATTCTTTCCCCTGCACTGT

330   For each sample, total DNA obtained from 4×10^7 cells was used as input with 10 μg DNA per

331   100 μl PCR reaction. DNA was amplified using Herculase II Fusion DNA Polymerase

332   (Agilent) according to the manufacturer's conditions with 2 μl Herculase II and 2.5 mM $MgCl_2$.

333   Annealing was performed at 55°C and a total of 24 cycles. PCR reactions were cleaned up

334   using 0.8x AMPure beads (Beckman Coulter). NGS libraries were run on the Illumina

335   NovaSeq 6000 System generating 100 bp single-end reads.

336

337   Data analysis:

338   Demultiplexed reads were trimmed to exact 20 bp (sgRNA) using cutadapt. Subsequently, read

339   counts were assed using MAGeCK (v0.5.6) as well as sgRNA enrichment/depletion with

340   "mageck test -k *readcouts*.txt -t OT-I -c CTRL --norm-method control --control-sgrna

341   *nontargeting*.txt". For MAGeCK analysis three biological screening replicates were pooled.

342   For pathway analysis of gene enrichment/depletion the cut-off was set at FDR < 0.1 and GO

343   term analysis for candidates was performed using the Molecular Signature Database

344   (MSigDB). The screening data set can be found in Tables S1 and S2 and via the GEO accession

345   number GSE180834.

346

347   Isolation and activation of CD8 T-cells:

348    $CD8^+$ OT-I T-cells were isolated from spleen, axillary and inguinal lymph nodes from OT-I

349   mice. $CD8^+$ cells were enriched using magnetic beads for MACS (130-104-075, Milteny

350   Biotec). T-cells were cultured in IMDM supplemented with 10% fetal bovine serum (FBS),

351   1% penicillin/streptomycin (Gibco), 50 μM β-Mercaptoethanol (Gibco) and 100 ng/ml Il-2

352   (Peprotech). Cells were kept at 37°C in 5% CO_2. After T-cell isolation, cells were activated for

353   24h using 2 μg/ml of anti-Cd28 and anti-Cd3ε antibodies (102116 and 100340, BioLegend).

354

355   In vitro cytotoxicity assays:

356   One day prior to OT-I co-culture, a total of 5×10^4 Ovalbumin-expressing KPC cells were plated

357   into 24-well plates. For competition assays, KPC-Cas9-OVA-mCherry (with CRISPR-KO of

358   indicated gene) and KPC-Cas9-OVA-EGFP-sgRNA@ctrl were plated in a 1:1 ratio. Activated

359   OT-I T-cells were added in the presence of 100 ng/ml Il-2 for one to two days, depending on

360   downstream analysis. EGFP:mCherry ratio was assessed using flow cytometry. In brief, cells

361   were trypsinized, spun down and washed in FACS buffer (2% FBS, 2mM EDTA in PBS). For

362   MHC class I assessment, cells were detached using 5 mM EDTA. The following antibodies

363   were used: CD8a-APC (1:600), CD8a-FITC (1:600), H-2Kb-APC (1:100), SIINFEKL-H-2Kb-

364 APC (1:100; all Biolegend). SYTOX Blue was used as viability dye. For intracellular

365 Granzyme-B staining (GzmB-FITC; GB11; BioLegend) cells were stained with eFluor780

366 (fixable viability dye) and stained with 4% formalin before permeabilization. GzmB-FITC

367 staining was carried out in permeabilzation buffer for 30 min at room temperature. The

368 following sgRNAs were cloned into the LentiGuide-puro vector and stably integrated as a pool

369 per gene into target cells: *Ctrl-1*: 5' GCGAGGTATTCGGCTCCGCG, *Rnf31-1*: 5'

370 CTACCTCAACACCCTATCCA, *Rnf31-2*: 5' CCACCGTGCTGCGAAAGACG, *Rnf31-3*: 5'

371 TTCACTGAGCGCCAATACCG, *Vps4b-1*: 5' TAAAGCCAAGCAAAGTATCA, *Vps4b-2*:

372 5'CGATAGAGCAGAAAAACTAA, *Vps4b-3*: 5' TCAGGCCCAGTTGATGAGAA, *Stat1*:

373 5' GGATAGACGCCCAGCCACTG, *Atg5*: 5' AAGAGTCAGCTATTTGACGT.

374

375 Autophagy flux assay:

376 LC3-GFP-LC3ΔG-RFP construct was stably integrated into KPC-Cas9-OVA cells and

377 GFP[+]/RFP[+] single cell clones were sorted and expanded. Cells were starved for 8 hours in 2%

378 FBS/PBS at 37°C in ambient CO_2. Subsequently, cells were collected for flow cytometry

379 analysis in order to assess GFP and RFP expression. The autophagic flux was assessed by

380 calculating the GFP/RFP ratio and comparison to the non-starved control condition.

381

382 Human pancreatic cancer organoids:

383 Normal human pancreatic organoids (hPan) and pancreatic cancer organoids (hPDA) were

384 generated as described elsewhere [39]. Expansion medium (EM) contained Advanced

385 DMEM/F12 supplemented with 10 mM HEPES, 1x Glutamax, 1% Penicillin/Streptomycin, 1x

386 B27 without vitamin A (all Gibco), 1.25 mM N-acetylcysteine (Sigma), 25% WNT3A-

387 conditioned medium (CM), 10% RSPO1-CM, 10% NOGGIN-CM (all CM produced in-

388 house), 10 mM Nicotinamide (Sigma), 50 ng/mL human EGF (Peprotech), 100 ng/ml FGF10

389 (Peprotech), 10 nM Gastrin (Tocris Bioscience), 0.5 μM TGF-b type I receptor inhibitor A83-

390 01 (Tocris Bioscience) and 1μM PGE2 (Tocris Bioscience). Organoids were split every 7-10

391 days using TrypLE Express (Gibco) and fire-polished Pasteur pipettes in a 1:3 – 1:4 ratio. After

392 passaging, organoids were plated in 20 μl drops of Matrigel (Corning) and overlaid with EM

393 supplemented having 10 μM RhoKinase inhibitor (Y-27632; Abmole). Organoids from healthy

394 donors were lentivirally transduced to express oncogenic *KRAS*[G12V] and to knockout *TP53*

395 (hPan-KP). Both, hPan-KP and hPDA organoids were transduced with LentiCRISPRv2-puro

396 to knockout *RNF31*. For lentiviral transduction, 3 – 4 full drops of organoids per condition

397 were processed into single cells, mixed with 500 μl EM + 10 μM RhoKinase inhibitor + 50 μl

13

398   concentrated virus and spun for one hour at 32°C at 300 g in a 24-well plate. After 3 – 4 hours

399   incubation at 37°C, cells were collected and plated in Matrigel. Organoid were selected with

400   1.5 μg/ml puromycin (*RNF31*-KO), 10 μM Nutlin-3a (*TP53*-KO; Sigma) and 300 μg/ml

401   hygromycin (Kras^{G12V}). The following sgRNAs were used - *TP53*: 5'

402   GAAGGGACAGAAGATGACAG, *RNF31-1*: 5' CCACCGTGCTGCGAAAGACA, *RNF31-*

403   *2*: 5' CCCAACCCCTTACAGCCTCG, *RNF31-3*: 5' GGATCATGCTCACTAGCTGG.

404

405   Sublibrary generation:

406   For sublibrary generation, the top candidates (enriched and depleted; FDR < 10%) were

407   selected (Table S3). If there were many genes within one pathway, only a couple of genes was

408   selected to avoid redundancy. For each gene of the gene list (63 candidates and Ovalbumin) 10

409   sgRNAs (7 sgRNAs for Ovalbumin) were designed with the GPP sgRNA designer (Broad

410   Institute). A total of 600 non-targeting controls was likewise included. Oligonucleotides having

411   BsmBI (EspI) restriction sites, a single guide RNA sequence as well as primer binding sites for

412   oligo pool amplification were synthesized (Twist Bioscience). Oligo sequences can be found

413   in Table S3. PCR amplification of the oligo pool prior to cloning was done according to the

414   manufacturer's protocol. For cloning the oligo pool into the appropriate lentiviral backbone the

415   following reaction was set up: 5 μl 10x Cutsmart buffer (NEB), 1 mM DTT (final), 1 mM ATP

416   (final), 1.5 μl T4 DNA Ligase (8000U, NEB), 1.5 μl EspI (NEB), 100 ng oligo pool PCR

417   product and 500 ng vector (LentiGUIDE-puro, EspI-digested and isopropanol purified) and

418   water up to 50 μl. The reaction was incubated for 100 cycles at 5 min 37°C followed by 5 min

419   20°C. After isopropanol clean-up, the ligation was transformed into NEB Stable Competent *E.*

420   *coli* (C3040I) and streak out onto LB agar plates. Library integrity was confirmed using

421   Illumina sequencing.

422

423   In vivo sublibrary screen:

424   KPC-Cas9-OVA cells were transduced with the lentiviral sublibrary at a MOI of 0.3 and

425   selected for four days with 2 μg/ml Puromycin. Subsequently, 150.000 KPC-Cas9-OVA-

426   Sublibrary cells were orthotopically transplanted into Rag1$^{-/-}$ mice. On day 16 post

427   transplantation 1 x 10^6 preactivated OT-I CD8$^+$ T-cells were adoptively transferred

428   (intravenously) into tumor bearing mice. Mice were sacrificed on day 21 post transplantation

429   and tumors were harvested. Tumor DNA was isolated using the Qiagen Blood and Tissue Kit

430   and sgRNA cassette was amplified similarly to the *in vitro* screen and analyzed by Illumina

431   sequencing. Single guide RNA representation was assed using MAGeCK (v0.5.6) by

432   comparison to the plasmid sublibrary. The screening data set can be found in Table S3 and via

433   the GEO accession number GSE180834.

434

435   Transplantations:

436   Mice were anesthetized using isoflurane at a constant flow rate. Abdomen was shaved and

437   sterilized before small incision in the upper left quadrant was made. The pancreas was carefully

438   put onto a cotton-swab and 1.5 x10^5 KPC cells were injected in 50 μl of PBS:Matrigel (1:1)

439   using a 29G needle. Successful injection was confirmed when a liquid bled formed and no

440   leakage could be observed. Peritoneum and skin were subsequently sutured with Vicryl violet

441   sutures (N385H, Ethicon) and secured with wound clips (FST). Approximately three weeks

442   post transplantations animals were sacrificed and tumors were isolated, weighed and processed

443   for subsequent analysis. For subcutaneous transplantations, C57BL/6 mice were injected with

444   1x10^6 KPC or KPC-Cas9 cells per flank mix in 1:1 PBS:Matrigel. Tumors were measured with

445   calipers and the volume was estimated via the equation $(LxW^2)/2$.

446

447   Flow cytometry for tumor microenvironment analysis:

448   For flow cytometry analysis orthotopic tumors were collected and minced into small pieces

449   before digestion in Collagense IV (6000 U/ml) and DNase I (200 U/ml) for one hour at 37˚C.

450   Cell suspension was filtered through a 40 μm cell strainer. For cytokine stainings, cells were

451   restimulated with PMA (100 nM), ionomycin (1 μg/ml) and monensin (2 μg/ml) for 3-4 hours

452   at 37˚C in complete IMDM medium (Gibco). Viability staining was performed using the

453   fixable viability dye eFluor780. Staining with fluorescent antibodies was carried out for 15 min

454   at 4˚C in the dark. After washing in FACS buffer (2 mM EDTA, 2 % FBS), cell suspension

455   was acquired using BD Fortessa and FlowJo software (Treestar).

456

457   Antibodies used for flow cytometry:

458   PD-1 FITC (J43; eBioscience), NK1.1 PE (PK136; eBioscience), CD3e PE-Dazzle594 (145-

459   2C11; BioLegend), CD3e PE (145-2C11; eBioscience), FoxP3 PerCP-Cy5.5 (FJK-16s;

460   eBioscience), CD8a PE-Cy7 (53-6.7; eBioscience), CD8a APC (53-6.7; eBioscience), CD8a

461   PerCP-Cy5.5 (53-6.7; eBioscience), TCRb AF700 (H57-597; BioLegend), CD45 BV785 (30-

462   F11; BioLegend), CD4 BV711 (GK1.5; BioLegend), CD19 BV650 (6D5; BioLegend), CD19

463   PE (1D3; eBioscience), CD11b BV605 (M1/70; BioLegend), CD11b BV510 (M1/70;

15

464   BioLegend), CD11c BV605 (N418; BioLegend), Siglec-F PE (E50-2440; BD Biosciences),
465   F4/80 APC (BM8; BioLegend), Ly-6G AF 700 (1A8; BioLegend), MHC II BV650
466   (M5/114.15.2; BioLegend), CD64 BV421 (X54-5/7.1; BioLegend), TNF FITC (MP6-XT22;
467   BioLegend), IFNg PE-Cy7 (XMG1.2; BD Biosciences), GzmB FITC (GB11; BioLegend).
468   Gating strategy is depicted in Supplementary Figure 6d.

469

470   RNA-Seq:
471   After 6h of co-culture, OT-I T-cells and KPC-Cas9-OVA cancer cells were sorted using the
472   BD Aria cell sorter. KPC cells expressed mCherry, T-cells were stained with CD8a-APC (clone
473   53-6.7; Biolegend 100711) to separate both populations. RNA was isolated with the Qiagen
474   RNeasy Mini Kit and sent to the Functional Genomic Center Zurich (FGCZ) for standard
475   library preparation and Illumina sequencing. Reads were trimmed using cutadapt and mapped
476   to the mouse genome GRCm38 with HISAT2 followed by sorting using samtools. The raw
477   count matrix was generated in RStudio using Rsubread. Differential gene (DE) expression
478   analysis was performed with EdgeR and differentially expressed genes (LFC $\pm$ 1; FDR < 0.1)
479   were used as input for GO term analysis using the Molecular Signature Database (MSigDB).
480   RNA-Seq data can be accessed via GEO.

481

482   TNF treatment of KPC cells:
483   KPC cells were treated 24h with the indicated TNF concentration and stained subsequently for
484   immunofluorescence (see below) or with crystal violet to assess cell viability (here in the
485   presence of 1 μg/ml Actinomycin D). Crystal violet dye was reconstituted in 10% acetic acid
486   and absorbance was measured at 595 nm.

487

488   Immunofluorescence of KPC cells:
489   Cells were grown on glass cover slips, treated with TNF (100 ng/ml) and fixed for 10 minutes
490   at room temperature in 4% PFA. Cells were permeabilized and blocked in 0.5% Triton-X, 5%
491   normal donkey serum in PBS. Cleaved caspase 3 antibody (1:400, Cell signaling Technology,
492   9664) was diluted in blocking solution and incubated overnight at 4°C. Coverslips were washed
493   in PBS and incubated 2h at room temperature with secondary antibody (Donkey anti-rabbit-
494   568, ThermoFisher Scientific, 1:400) and DAPI. Coverslips were mounted with Prolong Gold
495   (ThermoFisher Scientific) and imaged with a Lunaphore.

496

497   Whole mount staining of human pancreatic cancer organoids:

498   Wildtype or *RNF31*[KO] hPan/hPDA organoids were treated for 4h with 100 ng/ml human TNF

499   (Peprotech) in 8-well μ-slides (Ibidi). After fixation in 4% PFA, organoids were blocked and

500   permeabilized in blocking solution (10 % normal donkey serum; 0.5% Triton-X in PBS). All

501   antibody incubations were performed overnight at 4°C on a rocking platform. Primary

502   antibodies: E-Cadherin (1:500, R&D Systems, AF748), cleaved Caspase 3 (1:400, Cell

503   Signaling Technology, 9664). Donkey-anti-goat 488 and donkey-anti-rabbit 568 were used as

504   secondary antibodies and counterstained with DAPI. Organoids were mounted with ProLong

505   Gold. Confocal Images were taken with a Zeiss LSM 880 Airyscan.

506

507   Western Blot:

508   Whole cell lysates were prepared in RIPA buffer (50mMTris-HCl pH 8.0, 150mMNaCl, 0.1%

509   SDS, 0.5% Na-Deoxycholate, 1%IGEPAL CA-630) supplemented with PhosSTOP

510   phosphatase inhibitors and cOmplete protease inhibitor cocktail (both Roche). BCA protein

511   assay (ThermoScientific) was used for protein quantification. Samples were loaded on 4%–

512   15% precast polyacrylamide gels (Bio-Rad) and transferred to PVDF (Bio-Rad) membranes in

513   Towbin buffer. Membranes were blocked in 5% Bovine Serum Albumin (Applichem) and

514   incubated overnight in primary antibodies phospho-p65 (1:1000; CST#3033), Caspase 8

515   (1:1000; CST#4790), cleaved Caspase 8 (1:1000, CST#8592) and Gapdh (1:3000;

516   CST#14C10). IRDye800CW and 680RD donkey anti-rabbit secondary antibodies were used

517   for detection (LI-COR). Protein bands were visualized with the ODYSSEY CLx imaging

518   system (LI-COR).

519

520   Statistics:

521   To compare data from experiments we either applied student's unpaired, two-tailed T-test or

522   One-Way ANOVA analysis, as indicated in the respective figure legend. A minimum of three

523   independent biological replicates was performed per experiment. P values less than 0.05 were

524   considered significant and significance levels were set as follows: *p < 0.05, **p < 0.01, ***p

525   < 0.001. Statistical comparisons were performed using RStudio and GraphPad Prims 9.

526

527   **Data and materials availability:**

528   RNA-Seq data and CRISPR screening data have been made accessible via GEO: GSE180834.

529   KPC cell line was received from Ximbio (Cat# 153474), including a materials transfer

530   agreement.

531

532

533

534

535   **Acknowledgement:**

536   We thank the Flow Cytometry Facilities of the University of Zurich and the ETH Zurich. Also,

537   we thank the Functional Genomics Center Zurich and the ETH Phenomics Center for their

538   support and infrastructure.

539

546

547   **Author Information:**

548   N.F. and G. S. conceptualized the study, performed experiments, analyzed the data and wrote

549   the manuscript. L.T. designed, supervised and analyzed flow cytometry experiments and gave

550   valuable input throughout the course of the project. S.J. helped analyzing RNA-Seq data. D.E.,

551   K.F.M., T.R. and F.A. performed experiments. N.F. and G.S. wrote the manuscript, L.T. and

552   M.K. reviewed and edited the manuscript. G.S. supervised the study. G.S. and M.K. acquired

553   funding. All authors approved the final version of the manuscript.

554

555   **Competing interests:** Authors declare that they have no competing interests.

556

557   **Supplementary Information:**

558   Supplementary Figures 1 – 6

559   Supplementary Tables 1 – 3

560   Supplementary References

561

562

References:

1. Zhang, Y., Crawford, H. C. & Pasca Di Magliano, M. Epithelial-Stromal Interactions in Pancreatic Cancer. (2018). doi:10.1146/annurev-physiol-020518

2. Zhang, Y. *et al*. Regulatory T cell depletion alters the tumor microenvironment and accelerates pancreatic carcinogenesis. Running title: Treg depletion accelerates pancreatic carcinogenesis. *Author Manuscr. Publ. OnlineFirst* (2020). doi:10.1158/2159-8290.CD-19-0958

3. Royal, R. E. *et al*. Phase 2 trial of single agent ipilimumab (Anti-CTLA-4) for locally advanced or metastatic pancreatic adenocarcinoma. *J. Immunother.* **33**, 828–833 (2010).

4. Steele, N. G., Carpenter, E. S., Kemp, S. B. & Sirihorachai, V. R. ✉. Multimodal mapping of the tumor and peripheral blood immune landscape in human pancreatic cancer. *Nat. Cancer* (2020). doi:10.1038/s43018-020-00121-4

5. Yarchoan, M., Hopkins, A. & Jaffee, E. M. Tumor Mutational Burden and Response Rate to PD-1 Inhibition. *N. Engl. J. Med.* **377**, 2500–2501 (2017).

6. Juneja, V. R. *et al*. PD-L1 on tumor cells is sufficient for immune evasion in immunogenic tumors and inhibits CD8 T cell cytotoxicity. *J. Exp. Med.* **214**, 895–904 (2017).

7. Carpenter, E. S., Steele, N. G. & Pasca di Magliano, M. Targeting the Microenvironment to Overcome Gemcitabine Resistance in Pancreatic Cancer. *Cancer Res.* **80**, 3070–3071 (2020).

8. Hegde, S. *et al*. Dendritic Cell Paucity Leads to Dysfunctional Immune Surveillance in Pancreatic Cancer. *Cancer Cell* **37**, 289-307.e9 (2020).

9. Yamamoto, K. *et al*. Autophagy promotes immune evasion of pancreatic cancer by degrading MHC-I. *Nat. 2020* 1–6 (2020). doi:10.1038/s41586-020-2229-5

10. Lawson, K. A. *et al*. Functional genomic landscape of cancer-intrinsic evasion of killing by T cells. *Nature* **586**, 1–7 (2020).

11. Young, T. M. *et al*. *Autophagy protects tumors from T cell-mediated cytotoxicity via inhibition of TNF -induced apoptosis*. *Sci. Immunol* **5**, (2020).

12. Manguso, R. T. *et al*. In vivo CRISPR screening identifies Ptpn2 as a cancer immunotherapy target. *Nature* **547**, 413–418 (2017).

13. Pan, D. *et al*. *A major chromatin regulator determines resistance of tumor cells to T cell-mediated killing*. (2018).

596 14. Patel, S. J. *et al*. Identification of essential genes for cancer immunotherapy. *Nature*
597   **548**, 537–542 (2017).

598 15. Dong, M. B. *et al*. Dhx37 modulates CD8 T cell activation, cytokine production, and
599   cytotoxicity d DHX37 interacts with PDCD11 and influences NF-kB activity. (2019).
600   doi:10.1016/j.cell.2019.07.044

601 16. Dubrot, J. *et al*. In vivo screens using a selective CRISPR antigen removal lentiviral
602   vector system reveal immune dependencies in renal cell carcinoma. *Immunity* **54**, 571-
603   585.e6 (2021).

604 17. Shifrut, E. *et al*. Genome-wide CRISPR Screens in Primary Human T Cells Reveal
605   Key Regulators of Immune Function. *Cell* **175**, 1958-1971.e15 (2018).

606 18. Li, F. *et al*. In vivo epigenetic crispr screen identifies asf1a as an immunotherapeutic
607   target in kras-mutant lung adenocarcinoma. *Cancer Discov*. **10**, 270–287 (2020).

608 19. Doench, J. G. *et al*. Optimized sgRNA design to maximize activity and minimize off-
609   target effects of CRISPR-Cas9. *Nat. Biotechnol*. **34**, 184–191 (2016).

610 20. Vredevoogd, D. W. *et al*. Augmenting Immunotherapy Impact by Lowering Tumor
611   TNF Cytotoxicity Threshold. *Cell* **178**, 585-599.e15 (2019).

612 21. Biancur, D. E. *et al*. Functional Genomics Identifies Metabolic Vulnerabilities in
613   Pancreatic Cancer. *Cell Metab*. **33**, 199-210.e8 (2020).

614 22. Ishizuka, J. J. *et al*. Loss of ADAR1 in tumours overcomes resistance to immune
615   checkpoint blockade. *Nature* **565**, 43–48 (2019).

616 23. Wang, Y. *et al*. Down Regulation of c-FLIPL Enhance PD-1 Blockade Efficacy in B16
617   Melanoma. *Front. Oncol*. **9**, 857 (2019).

618 24. Luebke, T. *et al*. c-FLIP and CD95 signaling are essential for survival of renal cell
619   carcinoma. *Cell Death Dis*. **10**, 1–12 (2019).

620 25. Karin, N. CXCR3 Ligands in Cancer and Autoimmunity, Chemoattraction of Effector
621   T Cells, and Beyond. *Frontiers in Immunology* **11**, 976 (2020).

622 26. Zhang, C. *et al*. CXCL9/10/11, a regulator of PD-L1 expression in gastric cancer.
623   *BMC Cancer* **18**, (2018).

624 27. Tang, Y. *et al*. Linear ubiquitination of cFLIP induced by LUBAC contributes to TNF-
625   induced apoptosis. *J. Biol. Chem*. **293**, 20062–20072 (2018).

626 28. Hrdinka, M. & Gyrd-Hansen, M. Molecular Cell The Met1-Linked Ubiquitin
627   Machinery: Emerging Themes of (De)regulation. *Mol. Cell* **68**, 265–280 (2017).

628 29. Oikawa, D., Sato, Y., Ito, H. & Tokunaga, F. Linear ubiquitin code: Its writer, erasers,

629   decoders, inhibitors, and implications in disorders. *International Journal of Molecular*
630   *Sciences* **21**, 3381 (2020).

631   30.   Takahashi, Y. *et al*. An autophagy assay reveals the ESCRT-III component CHMP2A
632   as a regulator of phagophore closure. *Nat*. *Commun*. **9**, 1–13 (2018).

633   31.   Kaizuka, T. *et al*. An Autophagic Flux Probe that Releases an Internal Control. *Mol*.
634   *Cell* **64**, 835–849 (2016).

635   32.   Baginska, J. *et al*. Granzyme B degradation by autophagy decreases tumor cell
636   susceptibility to natural killer-mediated lysis under hypoxia. *Proc*. *Natl*. *Acad*. *Sci*. *U*.
637   *S*. *A*. **110**, 17450–17455 (2013).

638   33.   Chollat-Namy, M. *et al*. The pharmalogical reactivation of p53 function improves
639   breast tumor cell lysis by granzyme B and NK cells through induction of autophagy.
640   *Cell Death Dis*. **10**, 1–20 (2019).

641   34.   Milton, C. K. *et al*. A genome-scale CRISPR screen identifies the ERBB and mTOR
642   signaling networks as key determinants of response to PI3K inhibition in pancreatic
643   cancer. *Mol*. *Cancer Ther*. **19**, 1423–1435 (2020).

644   35.   Li, J. *et al*. Epigenetic and transcriptional control of the epidermal growth factor
645   receptor (EGFR) regulates the tumor immune microenvironment in pancreatic cancer.
646   *Cancer Discov*. **18**, CD-20-0519 (2020).

647   36.   Yuan, S. *et al*. Global regulation of the histone mark H3K36me2 underlies epithelial
648   plasticity and metastatic progression. *Cancer Discov*. CD-19-1299 (2020).
649   doi:10.1158/2159-8290.CD-19-1299

650   37.   Kearney, C. J. *et al*. Tumor immune evasion arises through loss of TNF sensitivity.
651   *Sci*. *Immunol*. **3**, eaar3451 (2018).

652   38.   Noman, M. Z. *et al*. *Inhibition of Vps34 reprograms cold into hot inflamed tumors and*
653   *improves anti-PD-1/PD-L1 immunotherapy*. (2020).

654   39.   Boj, S. F. *et al*. Organoid models of human and mouse ductal pancreatic cancer. *Cell*
655   **160**, 324–338 (2015).

656
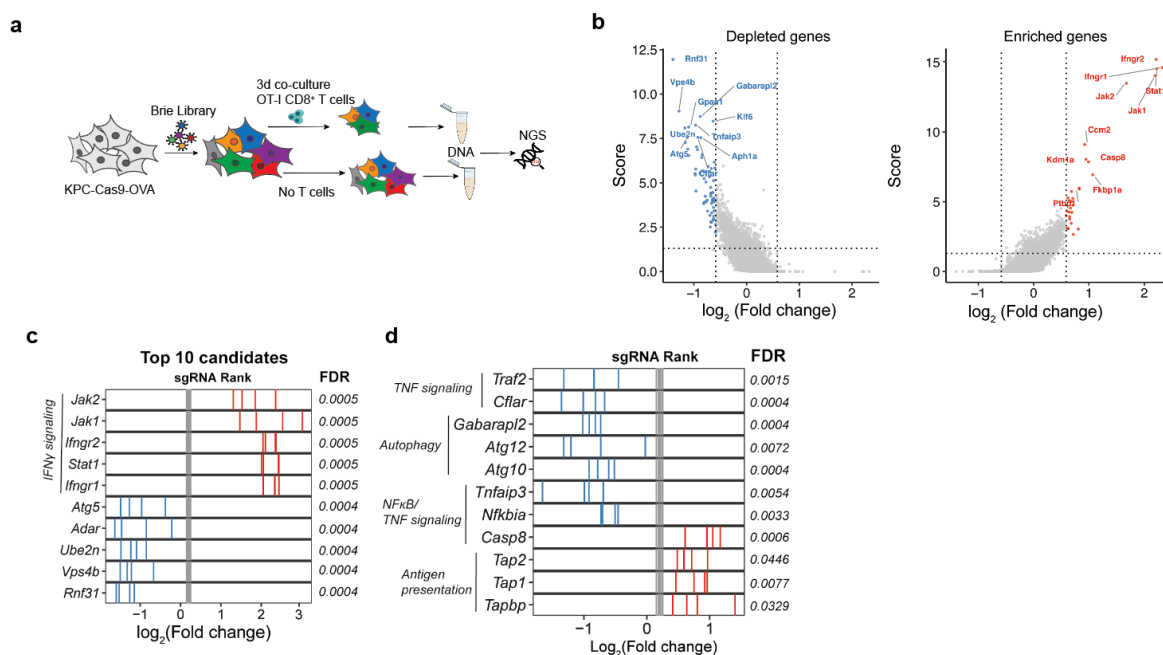
Figure 1: Genome-wide CRISPR screen in PDA cells reveals immune evasion mechanisms in vitro. (a) Schematic of genome-wide in vitro CRISPR screen. **(b)** Volcano plot of top ten depleted (blue) and enriched (red) genes. Screening analysis was performed with MaGeCK RRA. **(c)** sgRANK of the top (red) and bot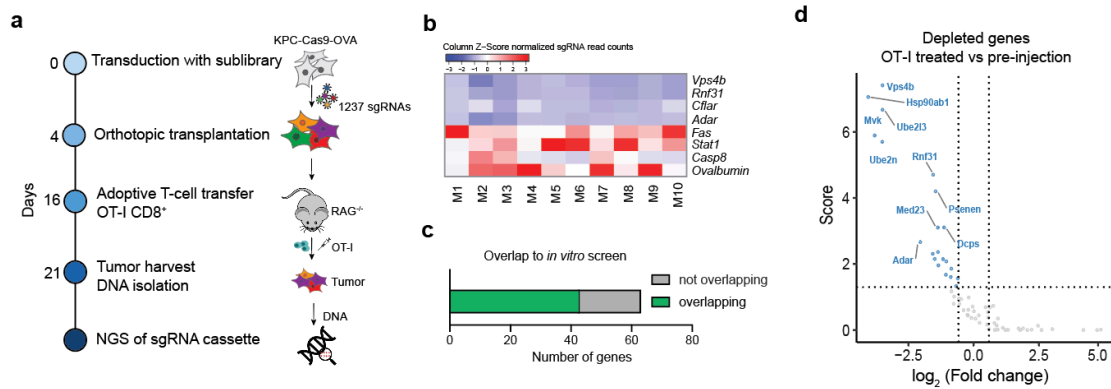tom (blue) five depleted genes is represented. Grey bars represent non-targeting sgRNAs. **(d)** sgRANK of the enriched (red) and depleted (blue) genes of different immune evasion pathways. Grey bars represent non-targeting sgRNAs.

667

Figure 2: A targeted CRISPR library screen validates candidates in vivo. (a) Schematic of the secondary CRISPR screen *in vivo*. **(b)** Heatmap of normalized read counts of sgRNAs across ten individual mice (M1 - M10). **(c)** Bar diagram of sublibrary genes in comparison to their predicted phenotype (from *in vitro* screen). **(d)** Volcano plot of depleted (blue dots) genes of the sublibrary *in vivo* screen when comparing the pool of preinjected KPC cells to OT-I CD8+ T cell treated tumors.

675
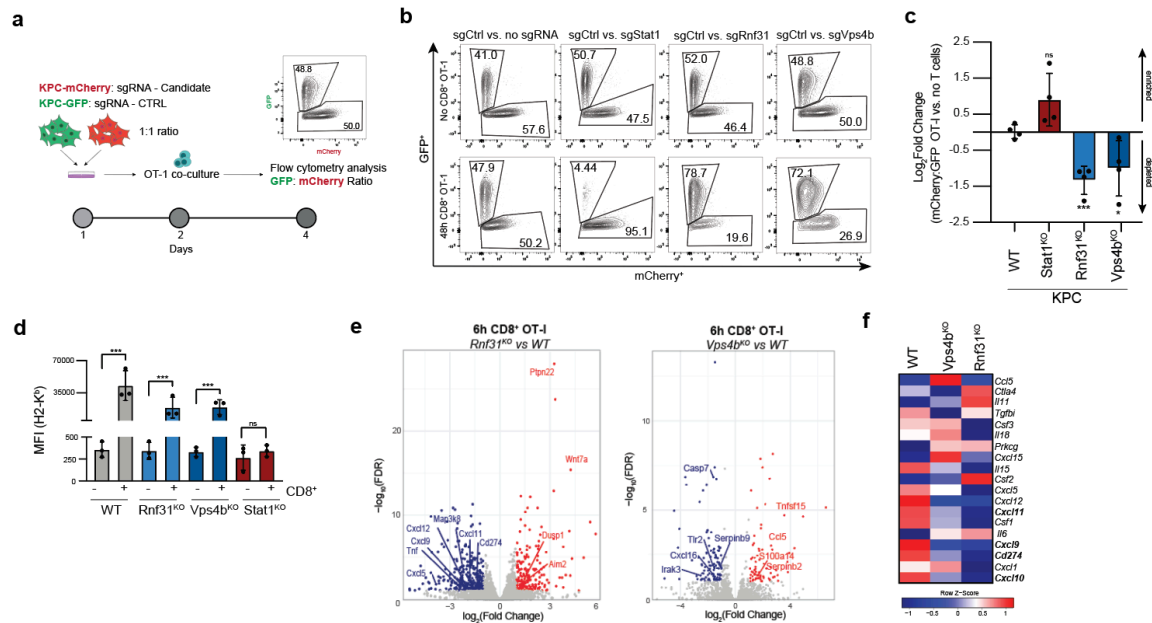
Figure 3: Arrayed validation of selected screening hits *in vitro*. **(a)** Schematic of *in vitro* competition assay. **(b)** Representative flow cytometry plots (GFP vs. mCherry) of the arrayed hit validation with and without T cell co-culture. **(c)** Quantification of **(b)**. Log$_2$ Fold change of the mCherry:GFP ratio OT-I treated compared to the matched untreated condition. **(d)** Mean fluorescence intensity (MFI) of Pan-H2-K^b. **(e)** Volcano plots of differentially expressed (DE) genes in *Rnf31*^{KO} and *Vps4b*^{KO} cells after 6h of OT-I T cell exposure compared to equivalently treated KPC^{WT} cells. Highlighted genes are putatively involved in anti-tumor immunity. DE genes in red/blue: | Log$_2$FC | > 1, FDR < 0.1. **(f)** Heatmap of normalized counts per million (CPM) of selected immune modulatory factors after OT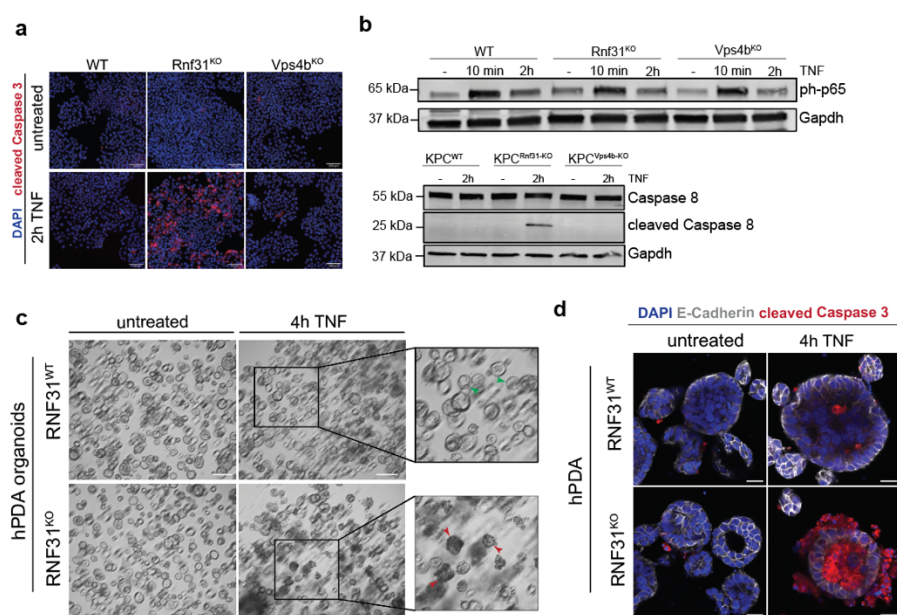-I T cell exposure across different genotypes. Significance in **(c)** was determined with an unpaired two-tailed t test. Significance in **(d)** was determined with one-way ANOVA analysis. *p < 0.05, **p < 0.01, ***p < 0.001; ns, non-significant, p > 0.05. Values represent mean $\pm$ SD, data are derived from at least three independent experiments.

689

690

Figure 4: *Rnf31*ᴷᴼ sensitizes PDA to TNF-triggered apoptosis. (a) Immunofluorescence staining of KPC candidate lines after 2h of 100 ng/ml TNF. Cleaved caspase 3 (red) and DAPI (blue). Scale bar represents 100 μm. **(b)** Western Blot analysis of KPC cell lines after TNF treatment (100 ng/ml) for active NFκB signaling (phospho-p65; upper panel) and cleaved caspase 8/caspase 8 (bottom panel). Gapdh was included as loading control. **(c)** Brightfield images of human PDA organoids in the presence of 100 ng/ml TNF for 4h. Boxes highlight viable (green arrows) and dying organoids (red arrows). Scale bar represents 200 μm. **(d)** Whole mount staining of human PDA organoids after 4h TNF (100 ng/ml) treatment with cleaved caspase 3 (red), E-cadherin (white) and DAPI (blue). Scale bar represents 20 μm.

700
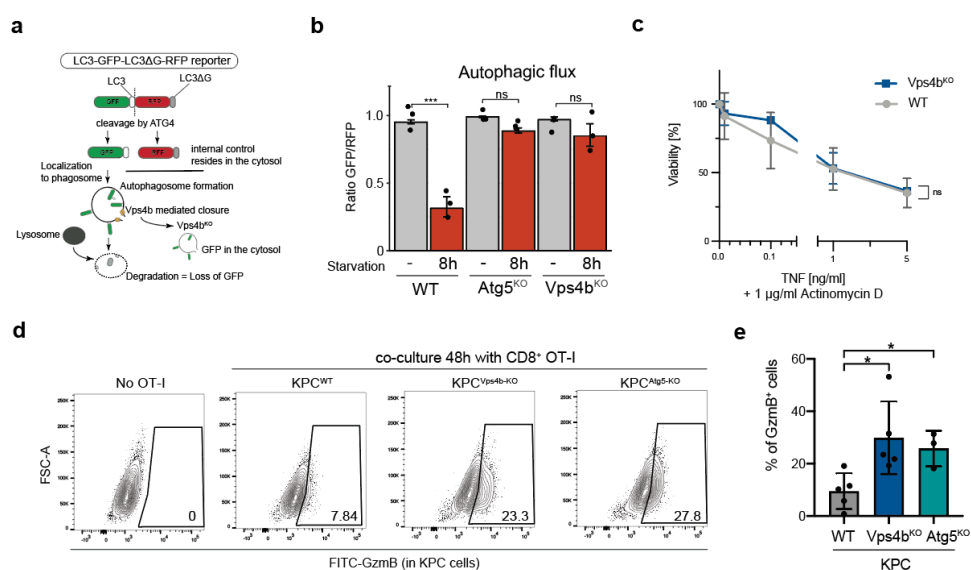
Figure 5: Disruption of Vps4b leads to impaired autophagy and granzyme B accumulation in tumor cells. (a) Schematic of autophagic flux reporter based on the LC3-GFP-LC3ΔG-RFP probe adapted from Kaizuka *et al*. [31]. **(b)** Quantification of autophagic flux by flow cytometry in different KPC lines under normal and starvation conditions (8h in PBS + 2% FBS). Bars represent the ratio of GFP to RFP expressing cells. **(c)** Assessment of TNF sensitivity threshold in WT and *Vps4b*[KO] KPC cells in the presence of 1 μg/ml actinomycin D. Crystal violet staining was used for quantification of viable cells. Represented data is relative to untreated control cells. **(d)** Flow cytometric analysis of intracellular granzyme B in KPC cells. Cells were gated on FSC/SCC – viability - CD8-negative. **(e)** Quantification of granzyme B positive cancer cells and T cells base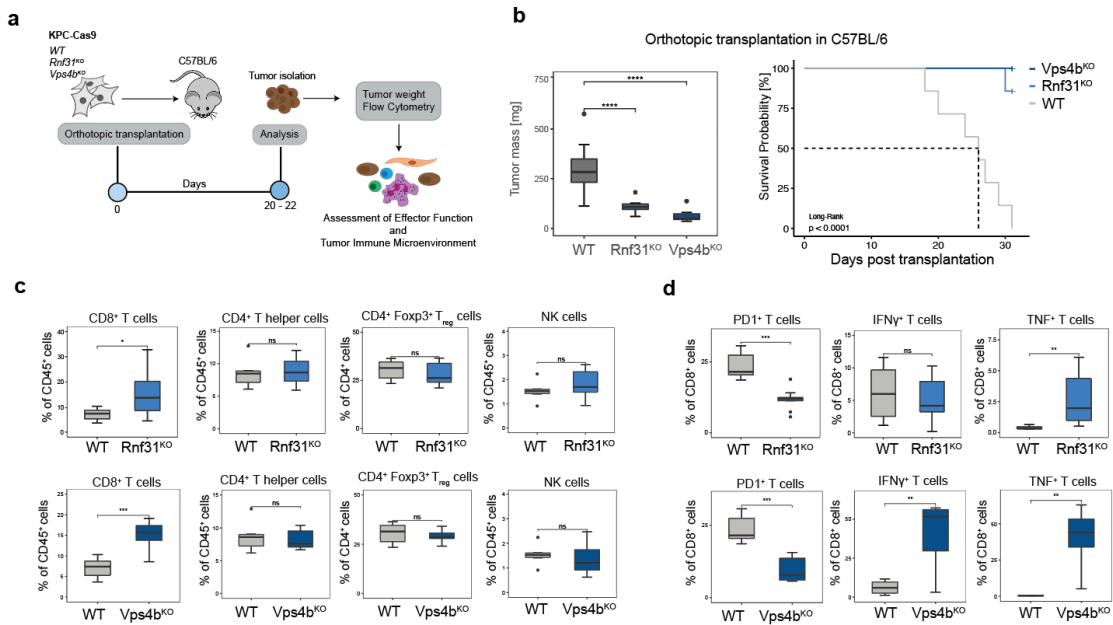d on **(d)**. Significance in **(c)** was determined with an unpaired two-tailed t test. Significance in **(b)** was determined with one-way ANOVA. Significance in **(e)** was determined with an unpaired, two-tailed t-test. *$p < 0.05$, **$p < 0.01$, ***$p < 0.001$; ns, non-significant, $p > 0.05$. Values represent mean $\pm$ SD, data are derived from at least three independent experiments.

27

Figure 6: *Rnf31*^KO^ and *Vps4b*^KO^ enhances CD8+ T cell function *in vivo*. (a) Schematic of in vivo experimental set up. **(b)** Tumor weight and survival after orthotopic transplantation into C5BL/6 mice. **(c)** Flow cytometry analysis of immune cell population within tumors. **(d)** Flow cytometry analysis of effector function of CD8+ T cells within tumors. Significance in **(b, panel 1)**, **(c)** and **(d)** was determined with an unpaired two-tailed t test. *$p < 0.05$, **$p < 0.01$, ***$p < 0.001$; ns, non-significant, $p > 0.05$. The middle line in the boxplots shows the median, the lower and upper hinges represent the first and third quartiles, and whiskers represent $\pm1.5\times$ the interquartile range.